AIAA-2000-3066

Networked Rectenna Array for Smart Material Actuators

Sang H. Choi[†], Walter T. Golembiewski[‡], and Kyo D. Song[‡]

NASA Langley Research Center
Hampton, Virginia 23681-2199

ABSTRACT

The concept of microwave-driven smart material actuators is envisioned as the best option to alleviate the complexity associated with hard-wired control circuitry. Networked rectenna patch array receives and converts microwave power into a DC power for an array of smart actuators. To use microwave power effectively, the concept of a power allocation and distribution (PAD) circuit is adopted for networking a rectenna/actuator patch array. The PAD circuit is imbedded into a single embodiment of rectenna and actuator array. The thin-film microcircuit embodiment of PAD circuit adds insignificant amount of rigidity to membrane flexibility. Preliminary design and fabrication of PAD circuitry that consists of a few nodal elements were made for laboratory testing. The networked actuators were tested to correlate the network coupling effect, power allocation and distribution, and response time. The features of preliminary design are 16-channel computer control of actuators by a PCI board and the compensator for a power failure or leakage of one or more rectennas.

INTRODUCTION

The simplicity of microwave-driven actuator system can reduce a total weight and fabrication cost of the system. Smart material that enables itself to undergo shape changes in a predictable way [1,2] is used for actuator applications. Piezoelectric actuators can be employed in many applications, such as adaptive surface of antenna or telescope. Recently, it was utilized in a surface compensation of inflatable reflector antenna [3]. The surface compensation technique is extremely crucial to the success of NASA's future missions [4-7] including the Next Generation Space Telescope (NGST) that will replace the existing Hubble Space Telescope so that deep infrared and visible images of the most distant stars in our universe can be imaged and studied.

The microwave-driven smart material actuator [8,9] is a new concept and was introduced as a shape control device for NASA's next generation space telescope (NGST), large flexible membrane antennas, and solar sails. It is a combined structure of a microwave rectenna patch and an actuator unit. Microwave delivers a power by wireless transmission and controls and autonomously activates a large array of actuators without using hard-wired control routines.

Since the rectenna was first introduced by W. C. Brown in the 1960's [10], it has been used for various applications such as microwave-powered helicopter [11], the Solar Power Satellite (SPS) [12] that converts solar energy to RF and beams down to large 2.45-GHz rectennas on Earth, the 4.5-meter wingspan airplane that was powered only by microwave energy [13], and the microwave-powered balloon with an electronically steerable phased array [14]. Recently, a lightweight patch rectenna was developed at NASA's Jet Propulsion Laboratory [15]. Its structure is composed of a square planar array of identical unit cells. Each cell contains a receiving antenna, filter and rectifier circuitry in its planar structure. Microwave coupling between each copper antenna patch and its underlying filter and rectifier circuit occurs in two orthogonal slots in the copper ground plane.

The power received by a rectenna patch may not be sufficient for mobilizing an actuator because of either the dispersion of microwave or the extensive

[†] Sr. Research Scientist, NASA Langley Research Center
[‡] Professors, Norfolk State University

power feed required for shape changes. For piezoelectric actuators, the breakdown voltage of Schottky barrier diode used in each individual rectenna is a limiting factor. Low power density and/or power demand are typical when microwave is considered. Otherwise, high energy and high frequency microwave sources that are bulky and heavy, thus inappropriate for space applications, must be used. The issues related to low power density of microwave and power demand can be alleviated by employing the concept of power allocation and distribution (PAD).

A hard-wired control circuit would be ideal for a system that is comprised of a few of actuators. If a system has numerous nodal points (i.e., a thousand or more) that require power feed and control, the wiring may not be the suitable solution due to the network complexity, the weight increase attributed to wired network, the complex gate switching of power and control networks, and the interdependency of power and control routines. However, these shortcomings may be alleviated by loosely coupled microwave beam steering action and by beam-tailoring using microwave properties such as power, frequency, and polarization.

Thousands of shape control nodes for large space antennas or aircraft morphing structures impose challenges for developing a control network matrix. Onboard power and control routines in a matrix control network create unbearable complexity for wiring and power infrastructure.

POWER ALLOCATION AND DISTRIBUTION

An array of the rectenna patches networked in a serial mode would provide a collected voltage that is required to drive actuators. The networked control logic in a PAD circuitry, in principle, operates to allocate whole DC power from a rectenna patch array to a certain region of actuator array where surface correction is commanded and then therein the power is distributed to each individual actuator based on power need. Hence, the power allocated to the needed area exceeds the threshold power level and energizes the actuators. The power density of microwave at a receiving area can be estimated by the Goubau relationship [16].

$$\tau = \frac{\sqrt{A_t A_r}}{\lambda Z},$$

where τ is 3.0 for 100% efficiency, A_t the aperture area of transmitting antenna, A_r the aperture area of receiving antenna, λ the wavelength of microwave, and Z the distance between two antenna. If the diameter of transmitting antenna is assumed as 0.2 m, the foot print of the microwave can be predicted at various frequencies as shown in Fig. 1. The exposed rectenna patch area of 50 GHz and 1 kW microwave at 50 meters away is approximately 3 meters in diameter. The power density available for rectenna patch is 14 mW/cm^2. After conversion through rectenna (with max. efficiency of 85 %), the DC power density is 12 mW/cm^2. The 1 cm^2 area rectenna with 14 volts breakdown-limit Schottky diodes generates 10 VDC with 1.2 mA current. With 1.2 mA DC current, a multilayer piezoelectric actuator (1.8 μF) would have 15 milliseconds response time which is slow. For a higher voltage output, a load resister is required but the conversion efficiency drops drastically (see Fig. 2). For 70 volts output (171 μA), the response time slows down badly to 0.7 seconds. This approach clearly bares up with penalties of low efficiency and poor response time. Accordingly, the PAD is a logically acceptable approach provided that voltage boost is implemented at the rear end of PAD. The PAD circuitry utilizes most of microwave power at rectenna's maximum efficiency and tailors power mode and boosts either output voltage or output current for actuator array. The power distribution to a designated group of actuators can be controlled by the external command signals. Fig. 3 shows an illustration for PAD concept. A network circuitry that interconnects control logic of all participating rectennas allocates power that is received by an individual rectenna of the array to a group of actuators from one location to another location. The networked allocation of power is also regarded as a process of the power amplification corresponding to the power needs for a group of actuators. Within the group of actuators, the power allocated to the group is distributed to each actuator of the group according to power need.

PAD Circuitry - Electric utilities have solved their problem of power distribution by constructing a power grid of high voltage lines crisscrossing the country. Thus, the first element in the design of a PAD circuit is to construct a power lattice or grid similar to a screen. The power distribution grid will have vertical lines referred to as columns and horizontal lines referred to as rows. These lines are constructed of electrically conducting material. An actuator is placed at the node or intersection of each vertical and horizontal line as shown in Fig. 4.

1)

Power to each actuator is fed from four directions. Such a system insures power being delivered to a given node if some (max. three) of the cross-links should break or be destroyed. If at least one line remains, power will continue to flow to the actuator. Even if all four break, power would still fed and

control all other nodes or actuators in the membrane.

The simplest possible component for power distribution would be a variable resistor. An electronic device that can function as a simple variable resistor is a MOSFET. Enhancement mode power MOSFET's are classified as voltage controlled devices since the drain current I_D is controlled by the magnitude of the gate to source voltage, V_{GS}. When V_{GS} is high typically 10 volts, the drain-to-source resistance falls to a very low value (typically less than 1 ohm). I_D is also limited by the impedance of the load and the magnitude of the drain supply voltage. Applying a low voltage across the gate-to-source, simply 0 volts, the drain-to-source resistance increases (typically several mega-ohms) and turns the MOSFET off. Thus one MOSFET can function as the control element to one piezoelectric displacement actuator.

The remaining problem is how to control or address each MOSFET. The control logic used to refresh DRAM in a personal computer can be used. The memory logic voltage, 0 or 5 volts, is stored in a capacitor inside the memory. This capacitor will discharge if not refreshed periodically. Rows and columns are energized systematically in a swept fashion to recharge the memory capacitors. In a similar fashion, individual nodes in the distribution power grid can be addressed if the corresponding row and column are driven high. This solution implies that we have a MOSFET with two identical gate inputs capable of turning off the MOSFET independently. In a true **AND** gate fashion, the MOSFET will only conduct when both gate inputs (row and column) are high.

Most discrete MOSFET's used today have one gate drive. In early days, dual gate MOSFET's were used in RF mixers and automatic gain controlled IF (intermediary frequency) stage electronics. With the fabrication of ever increasing complex integrated circuits, the low demand for dual gate FET's has forced many manufacturers to stop making them nowadays. We were only able to obtain discontinued Motorola dual-gate depletion mode MOSFETs, the MFE201. The depletion mode operation forced the control circuitry to use negative gate drive voltages in order to turn the MOSFET off.

A 4x4 PAD Circuit Fabrication - A 4 X 4 grid of MOSFET's was constructed by connecting all the number two gates (G2) of four MOSFET's together in the first row. Refer to Fig. 4 for construction details. A row activation pulse will be applied to all of the G2 gates in the first row (row 0) in order to activate the first row. In addition, all of the number one gates (G1) of the first MOSFET in each row are tied together. A different voltage will be applied to each column to drive each actuator in the row to a desired on condition. Thus, two electrically independent layers are formed. The first layer has all of the G2 gates tied together in four rows. Connecting all of the G1 gates together in four columns forms the second layer. It takes four row wires and four column wires to control sixteen MOSFET's and the corresponding actuators. This scheme can be extended to 10,000 actuators by 100 row connections and 100 column connections. The required number of row or column wires is given by the square root of the number of actuators.

Finally, in the design, a digital to analog converter board in a standard computer is used to turn on rows and columns wires in a round-robin fashion. A separate analog channel is used for each row or column. A Visual Basic program (Version 6.0) is used to control the digital to analog output board.

Visual Basic Control Program - First channel 8 of the DAC is changed from -5 volts (off condition) to 0 volts (on condition). Since it is tied to all of the G2 gates in the first row of actuators, the row zero becomes active. Next each channel 0 to channel 3 of the DAC is set to the voltage that the operator wants to apply to actuators 0 to 3. Each voltage level can be independently controlled because each channel 0 to 3 is tied to a separate G1 gate in row zero. Next channels 0 to 3 are sequenced off and finally channel 8 is turned off. The actuators in row 0 (the first row) are now charged to the appropriate voltage level.

Next channel 9 of the DAC (digital to analog output board) is changed from -5 volts (off condition) to 0 volts (on condition). Since it is tied to all of the G2 gates in the second row of actuators, the row 1 becomes active. Next each channel 0 to channel 3 of the DAC is set to the voltage that the operator wants to apply to actuators 4 to 7. Each voltage level can be independently controlled because each channel 0 to 3 is tied to a separate G1 gate in row 2. Next channels 0 to 3 are sequenced off and finally channel 9 is turned off. The actuators in row 1 (the second row) are now charged to the appropriate voltage level.

This sequencing continues with channel 10 and 11. When all sixteen actuators are charged, the basic program returns to channel 8 and row 0.

Actuator Equivalency - Piezoelectric actuators have a wide range of voltage requirements from 10 volts to 200 volts and generally low current requirements. In general, they are voltage-controlled

devices with an equivalent circuit of capacitors in series with resistors. The equivalent circuit is dominated by the capacitance value.

Our PAD design takes advantage of the capacitance of the actuators by pulse charging them during a short on cycle. If the actuator has a low level of leakage (a very good capacitor), it will maintain that voltage until it is recharged by the next on pulse. However, an ideal capacitor is a dual edged sword. If the actuator does not have sufficient leakage, then it can not drain the charge when the voltage across it needs to be reduced. In that case, a parallel resistor would have to be placed across the actuator.

To simulate the actuators for our test, we selected a 1.5 μF epoxy dipped solid tantalum capacitor. It was a standard value closest to a typical value of 1.8 μF used by others. The capacitors used in the laboratory typically had one to two microamps leakage at 10 volts. This equates to an internal shunt resistance of 5 to 10 megaohms across the capacitor. One time constant (RC) is approximately 7.5 seconds. Therefore, it can take 45 or more seconds to discharge the capacitor from 10 volts to near several hundred millivolts.

TEST RESULTS OF PAD CIRCUIT

Because only depletion-mode dual gate MOSFETs were available, negative voltages had to be applied to control the MOSFETs and actuators. The analog output board was capable of supplying negative as well as positive voltages. With -5 volts on G1 and -5 volts on G2 the MOSFET should be turned off. With the MOSFET turned off 15 millivolts were measured across the capacitor when the power grid was set to 10 volts. This voltage is developed by the leakage current flowing through the capacitor in series with the MOSFET leakage. The addition of a voltmeter or oscilloscope to measure the voltage across the capacitor would allow it to further discharge to a lower value. After a minute or two the voltage across the same capacitor (originally 15 millivolts) falls to 6 or 7 millivolts. In any real world deployment of a PAD system, designers will have to factor in some residual voltage remaining across the smart material due to leakage current. A better MOSFET may reduce that to an acceptable level, but it will always exist.

Fig. 5a shows the relationship between the first row activation pulse applied to G2 and the first column level pulse applied to G1. This figure shows the input to the MOSFET controlling actuator 0,0 in row 0, column 0. It takes about 50 microseconds for the D/A output board to turn on an output and 10 microseconds to turn it off. The manufacturer of the D/A board CyberResearch specified a maximum D/A settling time of 2 microseconds. The rise time for the output pulses was measured at 4 μs. The cause of the delay could be the computer operating system itself or the time needed by visual basic to interpret and execute commands.

Fig. 5b shows the relationship between the first row activation pulse applied to G2 and the second column level pulse applied to G1. This figure shows the input to the second MOSFET controlling actuator 0,1 in row 0, column 1. It takes about 100 μs for the D/A output board to turn on the second MOSFET in each row. What is surprising is that there is a 50-μs delay between the start of the row activation pulse and the start of each subsequent column level pulse.

Fig. 5c is the input to the third MOSFET controlling actuator 0,2. Fig. 5d is the input to the fourth MOSFET controlling actuator 5. Comparison of Figs. 5a and 5d shows that the pulse width of the column level pulse decreases from 200 μs to 80 μs. This effect may or may not be acceptable in a practical deployment of this PAD circuitry. Fig. 6 is a hand drawn composite of all the applied voltages to a row of actuators. All voltages are referenced to the same 300-μs row activation pulse applied to G2.

The composite timing of the input (four column voltages) to four actuators during a single 280-μs row activation pulse is shown in Fig. 6. A total of four row activation pulses is generated during the 1160 μs duty cycle of the digital to analog output board. During the complete duty cycle, each of the sixteen actuators will receive one charging pulse. Fig. 6 shows that during a row pulse of 280-μs four individual pulses are generated with a 50-μs delay and feed to MOSFET's in each column.

The MOSFET used had a controllable voltage range of -2.5 to -1 volts, and with the sixteen bit analog output board used for the experiment, that yielded about 5000 controllable voltage points. Fig. 7 visually displays a linear response of the actuator voltages versus the analog input voltages to the MOSFET.

Since the voltages applied to the actuators are a pulse, an AC ripple voltage is generated by the charging of the actuator capacitance and discharged through the internal shunt resistance of the actuators. To compensate for this ripple voltage, the internal resistance of the capacitance can be increased as shown in Fig. 8. The ripple signals were taken by a Hameg oscilloscope with shunt

resistances of (a) 0.47 MΩ, (b) 1.8 MΩ, and (c) 5.0 MΩ resistance. Fig. 8 demonstrates that higher resistance and lower capacitance reduces the ripple on the actuators. Other components that can reduce the ripple are a higher speed digital to analog board and a faster computer.

Fig. 9 shows the power allocation and distribution to sixteen actuators. For number 1 actuator the voltage on the actuator was measured to be 10 volts. Allocating the power to 2 actuators from 10-volt input resulted in a measurement of 5.0 volts for each actuator. Likewise the measuring process is continued up to sixteen actuators. The signal to noise ratio for this measurement process is about a million to one so that the output result does not show significant influence in terms of power leakage. However, steady state power consumption across 16 actuators shows not uniform output power for individual actuators as shown in Fig. 10.

PIEZOELECTRIC ACTUATORS AND RECTENNA PATCH

The patch rectenna used is composed of 9 unit cells, whose dimension is 1 cm × 1 cm, respectively. The 3×3 patch rectenna and its microstrip filter and rectifier circuit are shown in Fig. 11. The DC power generated by rectenna was utilized as a power source to activate a multilayer piezoelectric actuator that is composed of PZT material. Multilayer piezoelectric actuators have been used for high longitudinal displacement, fast response, low driving voltage, and high energy conversion efficiency [17]. The typical properties of the multilayer piezoelectric actuator are listed in Table 1.

Table 1. Typical properties of the multilayer piezoelectric actuator.

Mechanical	
Dimension (L×W×H), mm	5 × 5 × 18
Compressive Strength, N/m^2	8.8×10^8
Tensile Strength, N/m^2	4.9×10^6
Young's Modulus, N/m^2	4.4×10^{10}
Density, kg/m^3	7900
Electrical	
Capacitance, μF	1.80

TEST OF PATCH RECTENNA

A JPL 3×3 patch rectenna was characterized for various conditions, such as transmitted power, frequency, beam incident angle, beam polarization. A 100 kΩ-loaded rectenna was used in tests to apply a high voltage to the actuator and maximize its performance. In this case, we obtained up to 73 V DC, whereas the efficiency was only 12 % (see Fig. 2). The effect of frequency on rectenna performance was tested at a constant power, 1.1 W, when the patch rectenna was placed at 25 in. away from the feed horn. The maximum voltage of 73 V DC was produced at 8.6 GHz as shown in Fig. 12.

Fig. 13 shows the displacement of multilayer piezoelectric actuator powered by the rectenna's DC voltage output up to about 70 V. The nearly linear relationship between the displacement and the applied voltage signifies nearly constant d_{33} (= 0.157 [μm/V]) over a whole test range. At 50 V, the displacement was about 8.0 μm, which is much larger than the 5.6 μm that was obtained with the same level of AC voltage at 0.5 Hz. At this frequency, however, dielectric loss due to the high frequency is expected to be negligible. Thus, if rms value of AC voltage is considered instead of the peak-to-peak value, we obtain good agreement between the AC source at 0.5 Hz and the rectenna power, as shown in Fig. 13.

CONCLUSION

The experimental results indicate that the multilayer piezoelectric actuator can be successfully utilized with a wide degree of controllability when the 3×3 patch rectenna converts microwave energy to DC power that, in turn, drives the actuator. This concept eliminates the need for the hard-wiring of the smart actuators on the adaptive surfaces of a large space deployable reflectors or inflatable antennas. Hence, it could dramatically reduce the cost of distributed shape-control systems and find application in many future and technically challenging space missions. The conceptual design of PAD presented is a reasonable solution to the complexity of wiring many actuators in a smart material. The design presented is simple enough to imbed into a thin film microcircuit layer during the fabrication of the smart material. It may be possible to improve the response of the design in several ways. Smart actuators with lower capacitance would shorten the response time to the drive voltages. A different D/A converter may improve the response. Programming the computer in assembly language is another possibility. A computer with a faster clock would decrease the duty cycle and improve the overall response. In terms of power leakage, the input power required for individual actuators does not have a significant impact on over all power demand.

ACKNOWLEDGMENTS

This work was performed partially under the NASA grant (NCC1-280) to Norfolk State University.

REFERENCES

1. *1993 American Heritage College Dictionary*, 3rd edition (Houghton Mifflin).
2. I. V. Galaev, M. N. Gupta, and B. Mattiasson, "Use Smart Polymers for Biosepartions," *CHEMTECH*, No. 12, pp. 19-25, 1996.
3. T. K. Wu, "Piezoelectrically adjustable array for large reflector antenna surface distortion compensation," *Microwave and Optical Technology Letters*, Vol. 14, No. 4, pp. 221-224, 1997.
4. J. Huang, T. K. Wu, and S. W. Lee, "Tri-Band FSS with Circular Ring Elements," *IEEE Trans. Antennas Propagat.*, vol. AP-42, No. 2, pp. 166-175, 1994.
5. T. K. Wu, "Multiband FSS," in T. K. Wu (Ed.), *Frequency Selective and Grid Array*, John and Wiley & Sons, New York, 1995.
6. W. Schneider, J. Moore, T. Blankney, D. Smith, and J. Vacchione, "An Ultra-Lightweight High Gain Spacecraft Antenna," *IEEE Antennas Propagat. Int. Symp.*, Seattle, WA, June, pp. 886-889, 1994.
7. T. H. Lee, R. C. Rudduck, T. K. Wu, and C. Chandler, "Structure Scattering Analysis for SeaWinds Scatterometer Reflector Antenna Using Extended Aperture Integration and GTD," *IEEE Antennas propagat. Int. Symp.*, pp. 890-893, Seattle, WA, June, 1994.
8. Sang H. Choi, Lake, M., and Moore, C., "Microwave-driven Smart Material Actuators." Patent Pending, *NASA Case No. LAR 15754-1*, Feb 24, 1998.
9. Sang H. Choi, S. Chu, M. Kwak and A. D. Cutler, "A Study on a Microwave-driven Smart Material Actuator," *SPIE Symposium on Smart Structures and Materials*, 1999.
10. W. C. Brown, et al., *U.S. Patent 3 434 678*, Mar. 25, 1969.
11. W. C. Brown, "Experiments involving a microwave beam to power and position a helicopter," *IEEE Trans. Aerosp. Electron. Syst.*, Vol. AES-5, No. 5, pp. 692-702, 1969.
12. W. C. Brown, "Solar Power Satellite Program Rev. DOE/NASA Satellite Power System Concept Develop. Evalation Program," *Fianl Proc. Conf.* 800491, 1980.
13. J. Schlesak, A. Alden and T. Ohno, " A microwave powered high altitude platform," IEEE MTT-S Int. Microwave Symp. Dig., pp. 283-286 1988.
14. W. C. Brown, "Design study for a ground microwave power transmission system for use with a high-altitude powered platform," *NASA Final Contractor Report 168344*, Raytheon Rpt. PT-6052, 1983.
15. NASA JPL, "Patch Rectenna for Converting Microwave to DC Power," *NASA Tech Briefs*, Vol. 21, January, p. 40, 1997.
16. Brown, W. C., Draft of Paper Prepared for Presentation at the 8th Biennial SSI/Princeton Conference on Space Manufactureing, May 6-9, 1987.
17. K. Lubitz and H. Hellebrand, "Properties of PZT Multilayer Actuators," *IEEE 7th Inter. Symp. Applications of Ferroelectrics*, pp. 509-512, 1991.

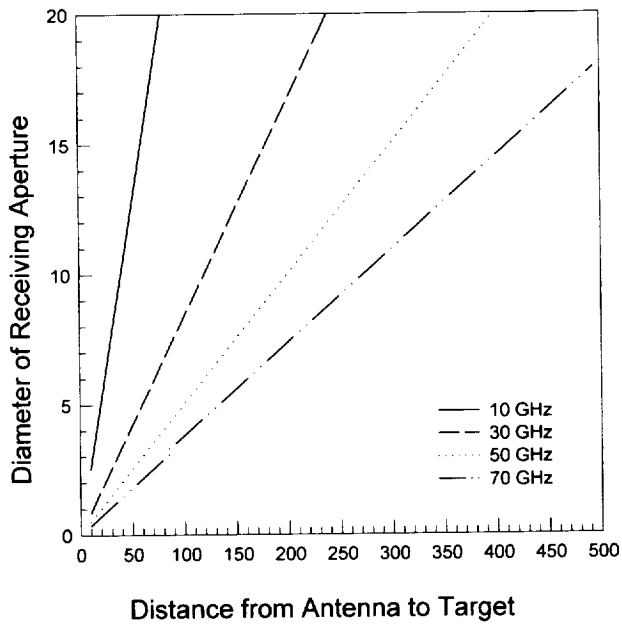

Fig. 1. Goubau Relationship (D = 18", η= 100%, τ = 3)

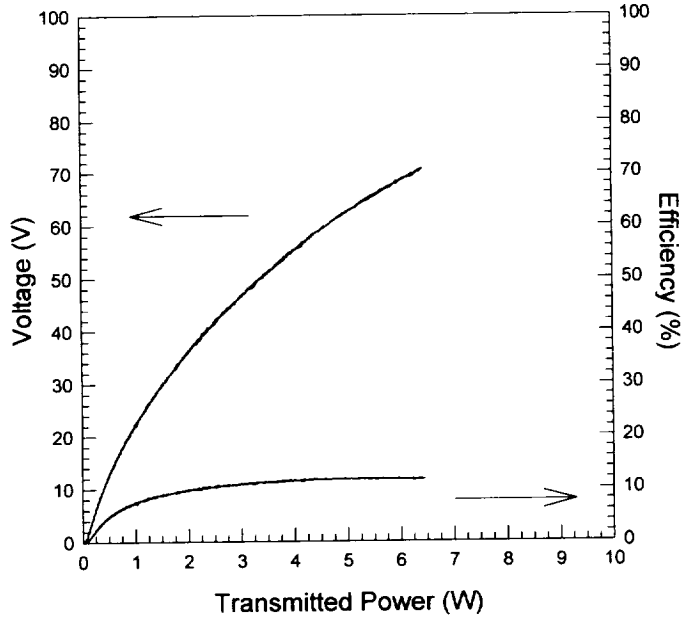

Fig. 2. Transmitted power effect on voltage output and efficiency obtained by 3x3 patch rectenna with 100,000 Ohm at 15" from feed horn at constant frequency of 8.5 GHz.

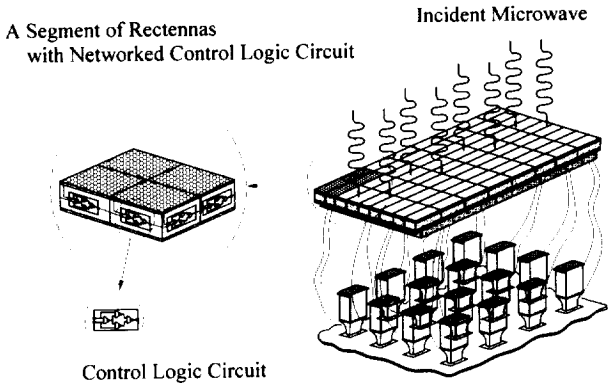

Fig. 3. A schematic diagram of networked control logic that is embedded into individual rectenna patch.

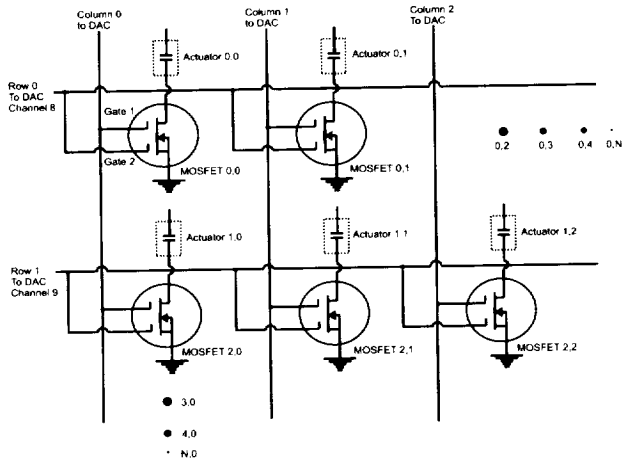

Fig. 4. A circuit diagram of power allocation and distribution (PAD).

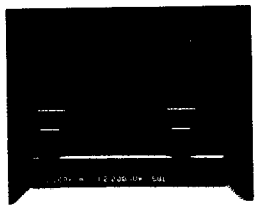

Fig. 5a Row 0, Column 0 MOSFET Input

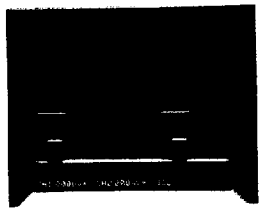

Fig. 5b Row 0, Column 1 MOSFET Input

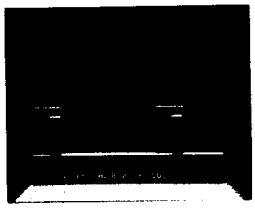

Fig. 5c Row 0, Column 2 MOSFET Input

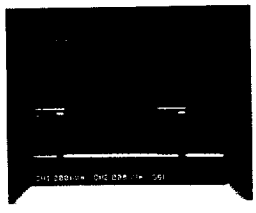

Fig. 5d Row 0, Column 3 MOSFET Input

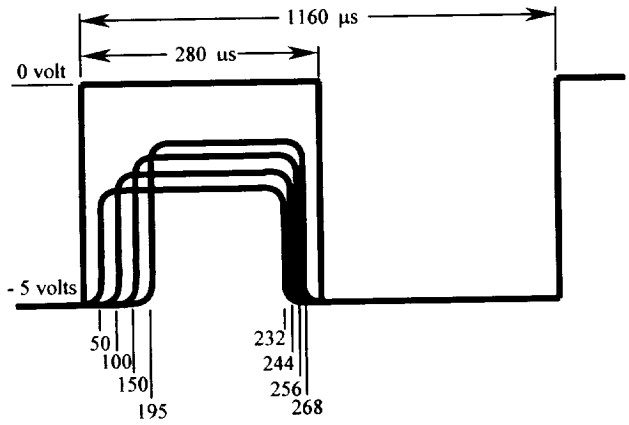

Fig. 6 Composite timing of column inout voltages and row actuation pulse

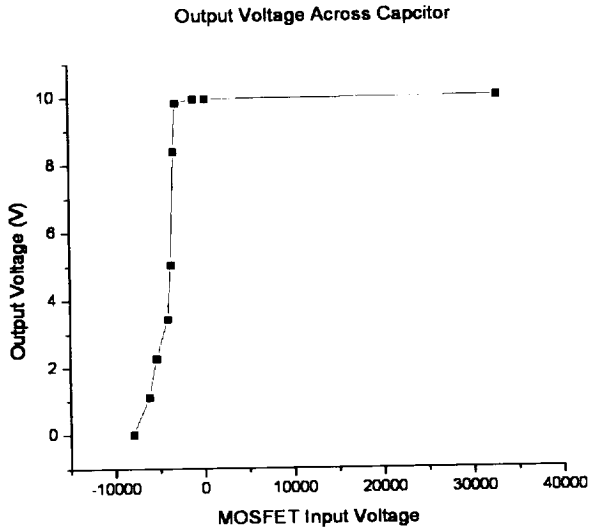

Fig. 7. Output voltage across capacitor

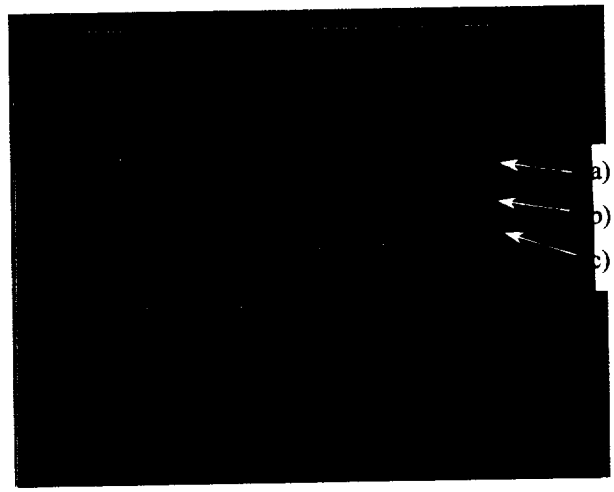

Fig. 8. Typical AC output voltages across actuators

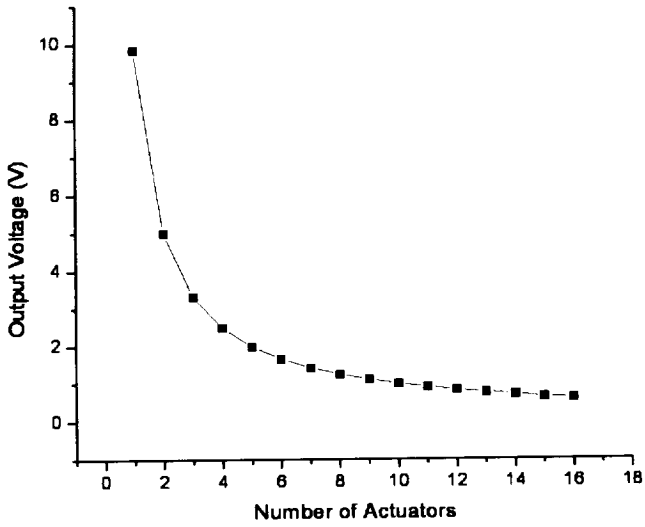

Fig. 9. Power level allocated to group of actuators

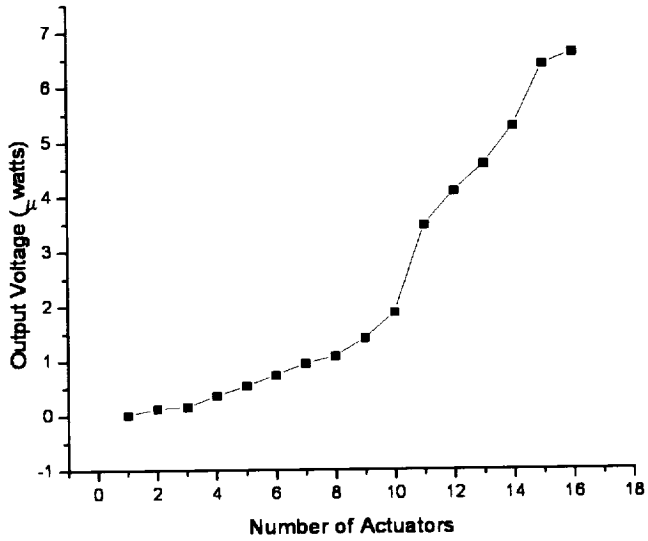

Fig. 10. Steady state power consumption across 4 x 4 actuators

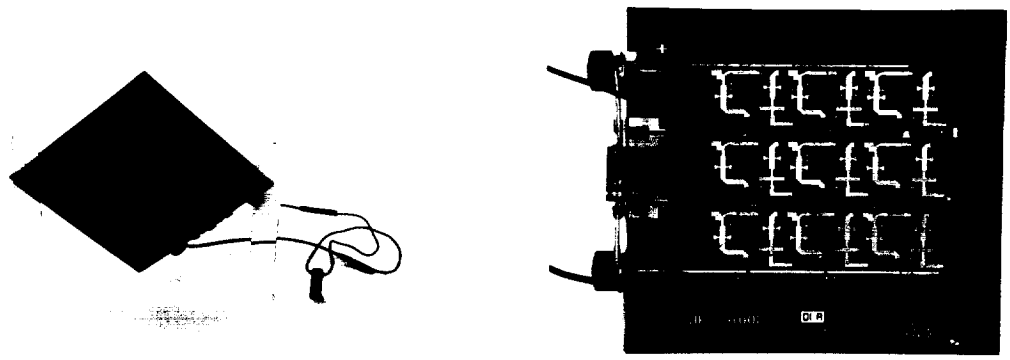

(a) (b)

Fig. 11. The photograph of JPL 3x3 patch rectenna: (a) the rectenna with the multilayer piezoelectric actuator and (b) microstrip filter and rectifier circuit.

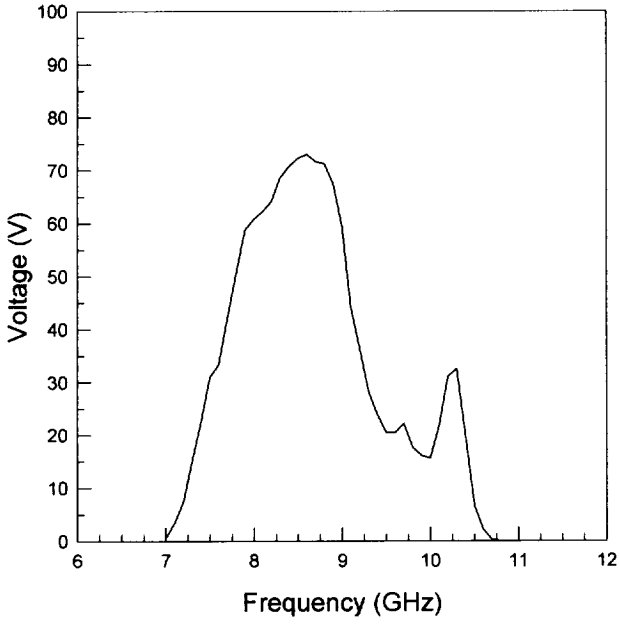

Fig. 12. Frequency effect on voltage output generated by 3x3 patch rectenna (100,000 Ohm) at 25" from feed horn with constant transmitted power of 1.1 W.

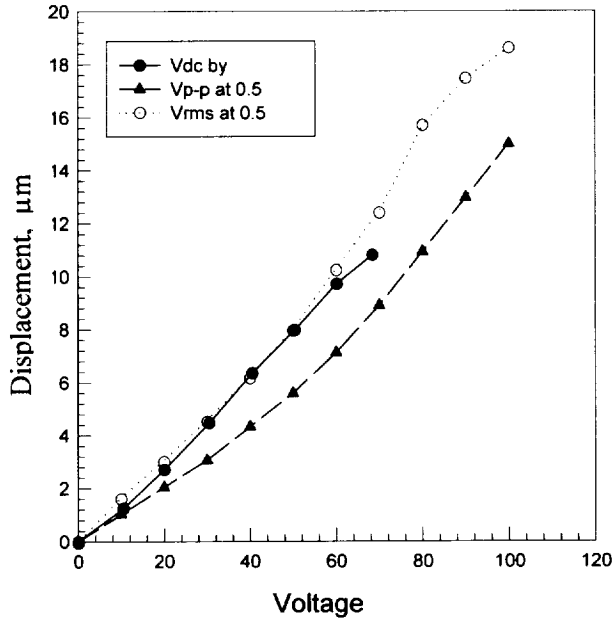

Fig. 13. Displacement of multilayer piezoelectric actuator activated by various power sources.

August 16, 2000

NASA STI Acquisitions DAA Authorization

The following papers (copies enclosed) have been DAA approved as Unclassified, Publicly Available documents:

Meeting Presentations:

36th AIAA/ASME/SAE/ASEE Joint Propulsion Conf. & Exhibit, 7/17-19/2000, Huntsville, AL:
K. A. Deere: Computational Investigation of the Aerodynamic Effects on Fluidic Thrust...
L. J. Bement; *et al.*: Explosive Joining for the Mars Sample Return Mission

41st AIAA/ASME/AHS/ASC Struct., Structural Dyn. & Mat'l. Conf., 4/3-8/2000, Atlanta, GA:
J. H. Starnes; *et al.*: Structural Similitude and Scaling Laws for Plates and Shells...

35th Intersociety Energy Conversion Engineering Conf., 7/24-28/2000, Las Vegas, NV:
S. H. Choi; *et al.*: Networked Rectenna Array for Smart Material Actuators

AIAA Modeling & Simulation Technologies Conf., 8/14-17/2000, Denver, CO:
M. Uenking: Pilot Biofeedback Training in the Cognitive Awareness Training...

Fluids 2000, 6/19-22/2000, Denver, CO:
J. B. Anders: Biomimetic Flow Control

30th Int'l Conference on Environmental Systems, 7/10-13/2000, Toulouse, France:
J. W. Wilson; *et al.*: Neutrons in Space: Shield Models and Design Issues

SAE General Aviation Technology Conf. and Exposition, 5/9-11/2000, Wichita, KS:
D. Palumbo; *et al.*: Optimizing Sensor and Acutator Arryas for ASAC Noise Control

AIAA Atmospheric Flight Mechanics Conf., 8/14-17/2000, Denver, CO:
E. A. Morelli: Low Order Equivalent System Identification for the Tu-144LL Supersonic...

51st Int'l Astonautical Congress, 10/2-6/2000, Rio de Janeiro, Brazil:
W. M. Piland; *et al.*: Improving the Discipline of Cost Estimation and Analysis

18th Applied Aerodynamics Conf., 8/14-17/2000, Denver, CO:
M. A. Park; *et al.*: Steady - State Computation of Constant Rotational Rate Dynamic...

10th Int'l Symp. on App'l. of Laser Techn. to Fluid Mechanics, 7/10-13/2000, Lisbon, Portugal:
J. F. Meyers; *et al.*: Identification and Minimization of Errors in Doppler Global...

IRS2000 Int'l. Radiation Symposium, 7/24-29/2000, St. Petersburg, Russia:
B. Lin; *et al.*: Overcast Clouds Determined by TRMM Measurements